Article

Cell

Hypervulnerability to Sound Exposure through Impaired Adaptive Proliferation of Peroxisomes

Graphical Abstract

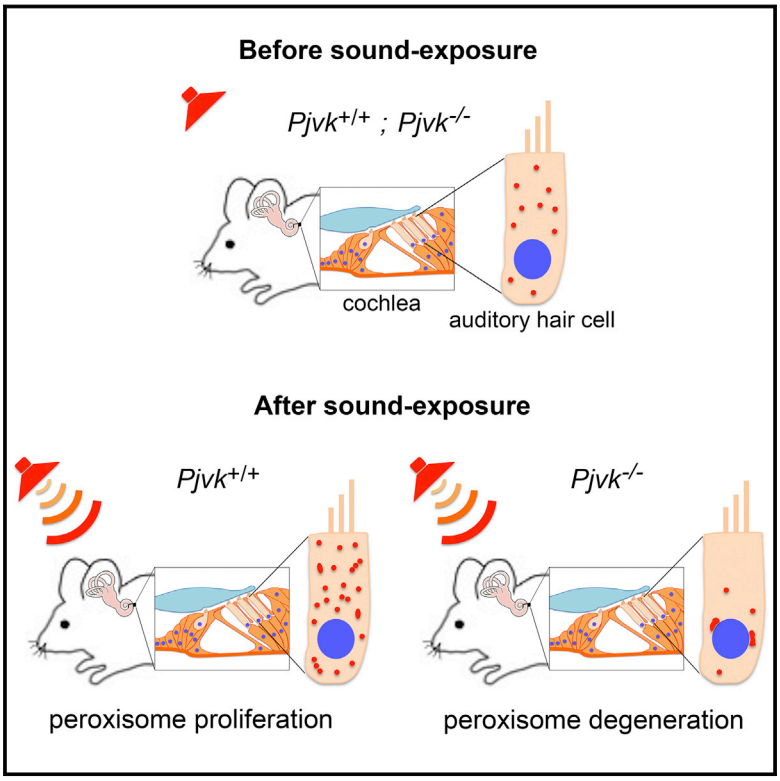

Authors

Sedigheh Delmaghani, Jean Defourny, Asadollah Aghaie, ..., Jean-Pierre Hardelin, Paul Avan, Christine Petit

Correspondence

christine.petit@pasteur.fr

In Brief

Hypervulnerability to sound exposure in pejvakin-deficient mice results from impaired adaptive proliferation of peroxisomes in response to the oxidative stress. In wild-type mice, loud sounds elicit adaptive peroxisomal proliferation.

Highlights

- Pejvakin-deficient mice and humans are hypervulnerable to sound exposure
- Oxidative stress induces a pejvakin-dependent proliferation of peroxisomes
- Peroxisome proliferation contributes to the physiological response to sound exposure
- *Pjvk* gene transfer can rescue auditory dysfunction in *Pjvk*$^{-/-}$ mice

Accession Number

GSE72722

Delmaghani et al., 2015, Cell *163*, 894–906
November 5, 2015 ©2015 Elsevier Inc.
http://dx.doi.org/10.1016/j.cell.2015.10.023

CellPress

Cell

Article

Hypervulnerability to Sound Exposure through Impaired Adaptive Proliferation of Peroxisomes

Sedigheh Delmaghani,[1,2,3] Jean Defourny,[1,2,3] Asadollah Aghaie,[2,3,4] Maryline Beurg,[5] Didier Dulon,[5] Nicolas Thelen,[6] Isabelle Perfettini,[1,2,3] Tibor Zelles,[7,8] Mate Aller,[7] Anaïs Meyer,[1,2,3] Alice Emptoz,[1,2,3] Fabrice Giraudet,[9,10,11] Michel Leibovici,[1,2,3] Sylvie Dartevelle,[12] Guillaume Soubigou,[13] Marc Thiry,[6] E. Sylvester Vizi,[7] Saaid Safieddine,[1,2,3] Jean-Pierre Hardelin,[1,2,3] Paul Avan,[9,10,11,15] and Christine Petit[1,2,3,4,14,15,*]

[1]Unité de Génétique et Physiologie de l'Audition, Institut Pasteur, 75015 Paris, France
[2]UMRS 1120, Institut National de la Santé et de la Recherche Médicale (INSERM), 75015 Paris, France
[3]Sorbonne Universités, UPMC Université Paris 06, Complexité du Vivant, 75005 Paris, France
[4]Syndrome de Usher et Autres Atteintes Rétino-Cochléaires, Institut de la Vision, 75012 Paris, France
[5]Equipe Neurophysiologie de la Synapse Auditive, Université de Bordeaux, Neurosciences Institute, CHU Pellegrin, 33076 Bordeaux, France
[6]Unit of Cell and Tissue Biology, GIGA-Neurosciences, University of Liege, CHU Sart-Tilman, B36, 4000 Liege, Belgium
[7]Institute of Experimental Medicine, Hungarian Academy of Sciences, 1083 Budapest, Hungary
[8]Department of Pharmacology and Pharmacotherapy, Semmelweis University, 1089 Budapest, Hungary
[9]Laboratoire de Biophysique Sensorielle, Université d'Auvergne, 63000 Clermont-Ferrand, France
[10]UMR 1107, Institut National de la Santé et de la Recherche Médicale (INSERM), 63000 Clermont-Ferrand, France
[11]Centre Jean Perrin, 63000 Clermont-Ferrand, France
[12]Plateforme d'Ingénierie des Anticorps, Institut Pasteur, 75015 Paris, France
[13]Plateforme Transcriptome et Épigénome, Institut Pasteur, 75015 Paris, France
[14]Collège de France, 75005 Paris, France
[15]Co-senior author
*Correspondence: christine.petit@pasteur.fr
http://dx.doi.org/10.1016/j.cell.2015.10.023

SUMMARY

A deficiency in pejvakin, a protein of unknown function, causes a strikingly heterogeneous form of human deafness. Pejvakin-deficient (*Pjvk*$^{-/-}$) mice also exhibit variable auditory phenotypes. Correlation between their hearing thresholds and the number of pups per cage suggest a possible harmful effect of pup vocalizations. Direct sound or electrical stimulation show that the cochlear sensory hair cells and auditory pathway neurons of *Pjvk*$^{-/-}$ mice and patients are exceptionally vulnerable to sound. Subcellular analysis revealed that pejvakin is associated with peroxisomes and required for their oxidative-stress-induced proliferation. *Pjvk*$^{-/-}$ cochleas display features of marked oxidative stress and impaired antioxidant defenses, and peroxisomes in *Pjvk*$^{-/-}$ hair cells show structural abnormalities after the onset of hearing. Noise exposure rapidly upregulates Pjvk cochlear transcription in wild-type mice and triggers peroxisome proliferation in hair cells and primary auditory neurons. Our results reveal that the antioxidant activity of peroxisomes protects the auditory system against noise-induced damage.

INTRODUCTION

Mutations of *PJVK*, which encodes pejvakin, a protein of unknown function present only in vertebrates, cause the DFNB59-recessive form of sensorineural hearing impairment. In the first patients described (Delmaghani et al., 2006), the impairment was restricted to neurons of the auditory pathway, with auditory brainstem responses (ABRs) displaying abnormally decreased wave amplitudes and increased inter-wave latencies (Starr and Rance, 2015). ABRs monitor the electrical response of auditory pathways to brief sound stimuli, from the primary auditory neurons synapsing with the sensory cells of the cochlea, the inner hair cells (IHCs), to the colliculus in the midbrain (Møller and Jannetta, 1983). However, some DFNB59 patients were found to have a cochlear dysfunction, as shown by an absence of the otoacoustic emissions (OAEs) that are produced by the outer hair cells (OHCs), frequency-tuned cells endowed with electromotility that mechanically amplify the sound stimulation of neighboring IHCs (Ashmore, 2008). These patients had truncating mutations of *PJVK*, whereas the previously identified patients, with extant OAEs, had missense mutations (p.T54I or p.R183W) (Ebermann et al., 2007; Schwander et al., 2007; Borck et al., 2012). However, the identification of patients also carrying the p.R183W missense mutation but lacking OAEs (Collin et al., 2007) refuted any straightforward connection between the nature of the *PJVK* mutation and the hearing phenotype. The severity of deafness in DFNB59 patients varies from moderate to profound

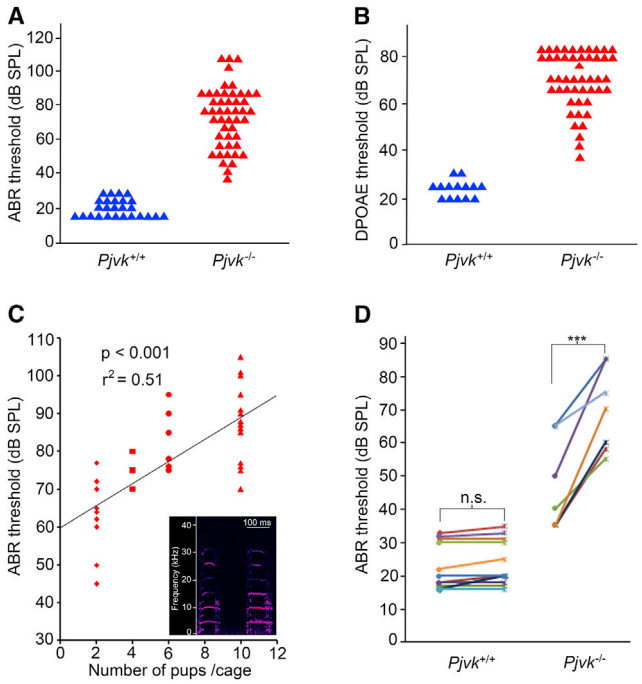

Figure 1. Hearing Loss Variability and Greater Sensitivity to Controlled Sound Exposure in *Pjvk*$^{-/-}$ Mice

(A) ABR thresholds at 10 kHz in P30 *Pjvk*$^{+/+}$ (n = 26 mice) and *Pjvk*$^{-/-}$ (n = 48 mice) littermates.

(B) DPOAE thresholds at 10 kHz in P30 *Pjvk*$^{+/+}$ (n = 14 mice) and *Pjvk*$^{-/-}$ (n = 48 mice) littermates. In ears with no DPOAE, even at 75 dB SPL (the highest sound intensity tested), DPOAE thresholds were arbitrarily set at 80 dB SPL.

(C) Relationship between the number of pups raised together (determining sound levels in the immediate environment) and ABR thresholds at 10 kHz in P21 *Pjvk*$^{-/-}$ pups. Inset: a time-frequency analysis of a mouse pup's vocalization. Pup calls from P0 to P21 form harmonic series of about 5 kHz, with the most energetic harmonic at about 10 kHz. In a 12-pup litter, call levels reach 105 ± 5 dB SPL at the entrance to the ear canals of the pups.

(D) ABR thresholds at 10 kHz in P30 *Pjvk*$^{+/+}$ and *Pjvk*$^{-/-}$ mice before (dots) and after (crosses) controlled sound exposure. ns, not significant; ***p < 0.001.

See also Figure S1.

and may even be progressive in some patients, suggesting that extrinsic factors may influence the hearing phenotype.

We investigated the role of pejvakin, with the aim of determining the origin of the phenotypic variability of the DFNB59 form of deafness. Our study of *Pjvk* knockout mouse models and of patients revealed an unprecedented hypervulnerability of auditory hair cells and neurons to sound exposure, accounting for phenotypic variability. We found that pejvakin is a peroxisome-associated protein involved in the oxidative-stress-induced proliferation of this organelle. Pejvakin-deficient mice revealed the key role of peroxisomes in the redox homeostasis of the auditory system and in the protection against noise-induced hearing loss.

RESULTS

Heterogeneity in the Hearing Sensitivity of *Pjvk*$^{-/-}$ Mice

We generated pejvakin-null (*Pjvk*$^{-/-}$) mice carrying a deletion of *Pjvk* exon 2, resulting in a frameshift at codon position 71 (p.Gly71*fs**9) (Figure S1; see the Supplemental Experimental Procedures). ABR thresholds recorded on postnatal day 30 (P30) *Pjvk*$^{-/-}$ mice (n = 48) ranged from 35 to 110 dB SPL (sound pressure level) at 10 kHz but never exceeded 30 dB SPL in their *Pjvk*$^{+/+}$ littermates (n = 26) (Figure 1A). This broad range of hearing sensitivity in *Pjvk*$^{-/-}$ mice, from near-normal hearing to almost complete deafness, extended across the whole frequency spectrum. The thresholds of distortion-product OAEs (DPOAEs) at 10 kHz (i.e., the minimum stimulus required for DPOAEs production by OHCs) also fell within an abnormally large range of values, from 30 to 75 dB SPL, in 28 *Pjvk*$^{-/-}$ mice, indicating an OHC dysfunction, and DPOAEs were undetectable in another 20 *Pjvk*$^{-/-}$ mice, suggesting a complete OHC defect (Figure 1B). The absence of pejvakin in mice thus results in a puzzlingly large degree of hearing phenotype variability.

Hypervulnerability to the Natural Acoustic Environment in *Pjvk*$^{-/-}$ Mice

We investigated the variability of *Pjvk*$^{-/-}$ auditory phenotypes, by first determining the ABR thresholds of *Pjvk*$^{-/-}$ littermates from different crosses. Large differences were observed between crosses, with much fewer differences between the *Pjvk*$^{-/-}$ littermates of individual crosses. Litters with larger numbers of pups (6 to 12) had higher ABR thresholds, suggesting that the natural acoustic environment, with the calls of larger numbers of pups, might be deleterious in *Pjvk*$^{-/-}$ mice. Pups are vocally very active from birth to about P20. We manipulated the level of exposure to pup calls by randomly splitting large litters of *Pjvk*$^{-/-}$ pups into groups of 2, 4, 6 and 10 pups per cage, with foster mothers, before P10, i.e., several days before hearing onset. The ABR thresholds at P21 were significantly correlated with the number of pups raised together ($p < 0.001$, $r^2 = 0.51$) (Figure 1C).

We then evaluated the effect of a controlled sound stimulation on hearing, by presenting 1,000 tone bursts at 10 kHz, 105 dB SPL (2-ms plateau stimulations separated by 60-ms intervals of silence), energetically equivalent to a 3-min stay in the natural environment of a 12-pup litter, while monitoring the ABRs during sound exposure. These conditions are referred to hereafter as "controlled sound exposure." We probed the effect of sound exposure by ABR tests, which, limited to 50 repetitions of tone bursts, did not influence the hearing thresholds of *Pjvk*$^{-/-}$ mice. In a sample of P30 *Pjvk*$^{-/-}$ mice with initial ABR threshold elevation (below 35 dB SPL), controlled sound exposure affected ABR thresholds in the 12–20 kHz frequency interval (corresponding to the cochlear zones in which hair-cell stimulation was strongest), with an immediate increase of 21.7 ± 10.3 dB (n = 8; p < 0.001), not observed in *Pjvk*$^{+/+}$ mice (2.2 ± 2.4 dB, n = 12; p = 0.3) (Figure 1D). *Pjvk*$^{-/-}$ mice transferred to a silent environment after exposure displayed a further increase of 33.7 ± 16.0 dB (n = 8) 2 days after exposure. The threshold shift decreased to 23.7 ± 18.0 dB at 7 days, and disappeared entirely by 14 days. When exposed mice were returned to the box with their littermates, their ABR continued to increase, at a rate of 15 dB per week. Pejvakin deficiency thus results in particularly high levels of vulnerability to low levels of acoustic energy, and the increase in ABR thresholds is reversible but only slowly and in a quiet environment.

Hair Cells and Auditory Pathway Neurons Are Affected by Pejvakin Deficiency

To identify the cellular targets of the pejvakin deficiency, we specifically probed the function of auditory hair cells and neurons in *Pjvk*$^{-/-}$, hair cell-conditional *Pjvk* knockout (*Pjvk*$^{fl/fl}$Myo15-*cre*$^{+/-}$), and *Pjvk*$^{+/+}$ mice, at the age of 3 weeks, before and after controlled sound exposure or controlled electrical stimulation. The responses of the IHCs to sound-induced vibrations amplified by OHCs trigger action potentials in the distal part of primary auditory neurons, at the origin of ABR wave I. In *Pjvk*$^{fl/fl}$Myo15-*cre*$^{+/-}$ mice, which lack pejvakin only in the hair cells, ABR wave I amplitude and latency at 105 dB SPL specifically probed IHC function, because IHC responses to such loud sounds are independent of OHC activity (Robles and Ruggero, 2001). The larger wave I latency (1.58 ms in *Pjvk*$^{fl/fl}$Myo15-*cre*$^{+/-}$ mice [n = 20] versus 1.32 ms in *Pjvk*$^{+/+}$ littermates [n = 30]; $p < 0.001$) and lower wave I amplitude (37% of the amplitude in *Pjvk*$^{+/+}$ littermates; $p < 0.001$) suggested a dysfunction of the IHCs. Controlled sound exposure induced further decreases in ABR wave I amplitude in *Pjvk*$^{-/-}$ and *Pjvk*$^{fl/fl}$Myo15-*cre*$^{+/-}$ mice (48% and 55% of pre-exposure amplitude, respectively) with respect to *Pjvk*$^{+/+}$ mice (108%; $p < 0.001$ for both comparisons) (Figure 2A), demonstrating that *Pjvk*$^{-/-}$ IHCs are hypervulnerable to sound. As shown above, OHCs are also affected by the pejvakin deficiency. Controlled sound exposure triggered a mean decrease in the DPOAE amplitude of 16.9 ± 7.2 dB in the 12 to 20 kHz frequency interval in *Pjvk*$^{-/-}$ mice with persistent DPOAEs (n = 8; $p < 0.0001$), and an increase in DPOAE threshold, but it had no effect on the DPOAEs of *Pjvk*$^{+/+}$ mice (n = 9; p = 0.51) (Figure 2B). OHCs lacking pejvakin are thus also hypervulnerable to sound.

We investigated the effect of the absence of pejvakin on the auditory pathway by comparing electrically evoked brainstem responses (EEBR) in *Pjvk*$^{-/-}$ and *Pjvk*$^{fl/fl}$Myo15-*cre*$^{+/-}$ mice (see the Supplemental Experimental Procedures). The amplitudes of the most distinctive EEBR waves, E II and E IV, did not differ between the two types of mice (for wave E IV: 2.6 ± 1.8 μV in *Pjvk*$^{-/-}$ mice [n = 18] and 2.2 ± 1.2 μV in *Pjvk*$^{fl/fl}$Myo15-*cre*$^{+/-}$ mice [n = 11]; t test, p = 0.13). However, following controlled electrical exposure at 200 impulses/s for 1 min, as opposed to electric-impulse stimulation with 16 impulses/s for 10 s for pre- and post-exposure EEBR tests, E II and E IV EEBR wave amplitudes got 41% and 47% smaller, respectively, for at least 3 min, in *Pjvk*$^{-/-}$ mice (n = 5; paired t test, p = 0.02 and p = 0.01, respectively), but were unaffected in *Pjvk*$^{fl/fl}$Myo15-*cre*$^{+/-}$ mice (n = 10; p = 0.83) (Figures 2D and 2G–2I). The E II-E IV interwave interval was 0.41 ms longer in *Pjvk*$^{-/-}$ mice (n = 5) than in *Pjvk*$^{fl/fl}$Myo15-*cre*$^{+/-}$ mice (n = 10; p = 0.003), and controlled electrical exposure extended this interval by a further 0.15 ms in *Pjvk*$^{-/-}$ mice only (paired t test, p = 0.001) (Figures 2H and 2I). Likewise, the latency interval between ABR wave I and wave IV (the counterpart of wave E IV), abnormal in one-third of the *Pjvk*$^{-/-}$ mice tested (with an ABR threshold < 95 dB SPL, n = 12) (Figures 2C and 2E), got abnormal in all of them after controlled sound exposure (0.16 ms further increase; paired t test, $p < 0.001$). By contrast, it remained normal in *Pjvk*$^{fl/fl}$Myo15-*cre*$^{+/-}$ mice (n = 10 ears; p = 0.73) (Figures 2C and 2F). Thus, the absence of pejvakin affects the propagation of action potentials in the auditory pathway after both controlled electrical and sound exposure in the *Pjvk*$^{-/-}$ mice.

To clarify whether these abnormalities were of neuronal or glial origin, we performed a rescue experiment in *Pjvk*$^{-/-}$ mice, using adeno-associated virus 8 (AAV8) vector-mediated transfer of the murine pejvakin cDNA (AAV8-Pjvk). AAV8 injected into the cochlea transduces the primary auditory neurons (cochlear ganglion neurons) and neurons of the cochlear nucleus (Figure S2A), but not the hair cells. All *Pjvk*$^{-/-}$ mice (n = 7) injected on P3 and tested on P21 had normal ABR interwave I-IV latencies (Figure 2J), and their EEBR wave-E IV amplitude was insensitive to controlled electrical stimulation (1.91 ± 0.97 μV before and 1.87 μV ± 1.07 after stimulation; paired t test, p = 0.59) (Figures 2K and 2L). The absence of pejvakin thus renders auditory pathway neurons hypervulnerable to exposure to mild, short sound stimuli.

Hypervulnerability to Sound in DFNB59 Patients

We then investigated whether the hearing of DFNB59 patients was also hypervulnerable to sound exposure. We tested five patients carrying the p.T54I mutation (Delmaghani et al., 2006). Transient-evoked OAEs (TEOAEs) assessing OHC function over a broad range of frequencies were detected for all ears, despite the severe hearing impairment (hearing threshold increasing from 66 dB HL at 250 Hz to 84 dB at 8 kHz). Following minimal exposure to impulse stimuli (clicks at 99 dB nHL), ABR waves were clearly identified in response to 250 clicks. When exposure was prolonged to 1,000 clicks (the standard procedure), wave V, the equivalent of mouse ABR-wave IV, which was initially conspicuous, displayed a decrease in amplitude (to 39% ± 30% of its initial amplitude) and an increase in latency (of 0.30 ± 0.15 ms) (Figures 3A, 3C, and 3D). In parallel, the I-V interwave interval increased by 0.30 ± 0.15 ms. Wave-V amplitude and latency recovered fully after 10 min of silence (Figure 3B). In control patients with sensorineural hearing impairment of cochlear origin matched for ABR thresholds, similar sound stimulation did not affect ABR wave-V amplitude (105% ± 14% of the initial amplitude after exposure; n = 13 patients) or latency (−0.02 ± 0.07 ms change after exposure) (Figures 3C and 3D). Exposure of the DFNB59 patients to 1,000 clicks also affected TEOAEs (6.1 ± 5.2 dB nHL decrease in amplitude; paired t test, p = 0.02). Therefore, as in pejvakin-deficient mice, the cochlear and neuronal responses of DFNB59 patients were affected by exposure to low-energy sound.

Redox Status Abnormalities and ROS-Induced Cell Damage in the Cochlea of *Pjvk*$^{-/-}$ Mice

We studied the *Pjvk*$^{-/-}$ cochlea by light microscopy on semithin sections and electron microscopy. On P15 and P21, both OHCs and IHCs were normal in number and shape. Their hair bundles (the mechanoreceptive structures responding to sound), the ribbon synapses of the IHCs, and their primary auditory neurons were unmodified (data not shown). On P30, we observed the loss of a few OHCs (16% ± 11%, n = 5 mice), restricted to the basal region of the cochlea (tuned to high-frequency sounds). From P30 onward, OHCs, cochlear ganglion neurons, and then IHCs disappeared, and the sensory epithelium (organ of Corti) progressively degenerated (Figure S3A).

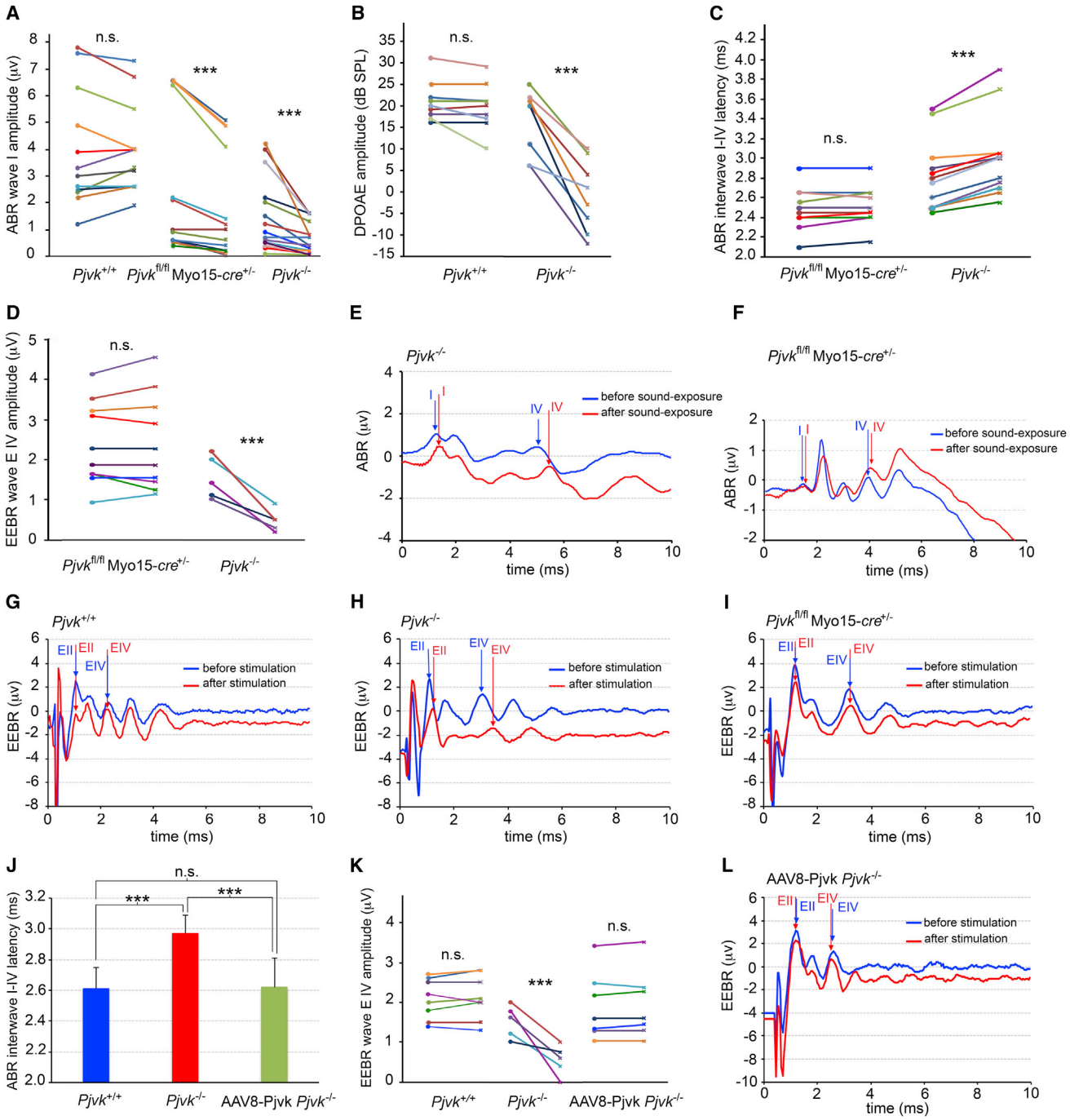

Figure 2. Effects on Auditory Function of Brief Exposure to Moderately Intense Stimuli in *Pjvk*$^{+/+}$, *Pjvk*$^{-/-}$, and *Pjvk*$^{fl/fl}$Myo15-*cre*$^{+/-}$ Mice

(A–C) ABR wave I amplitude (A), DPOAE amplitude (B), and ABR interwave I-IV latency (C) in *Pjvk*$^{+/+}$, *Pjvk*$^{-/-}$, and *Pjvk*$^{fl/fl}$Myo15-*cre*$^{+/-}$ mice, before (dots) and after (crosses) controlled sound exposure, revealing the hypervulnerability to sound of both types of cochlear hair cells (IHCs and OHCs) and of the neural pathway.

(D) EEBR wave E IV amplitude before and after controlled electrical exposure in *Pjvk*$^{-/-}$ and *Pjvk*$^{fl/fl}$Myo15-*cre*$^{+/-}$ mice was abnormal and hypervulnerable only when pejvakin is absent from auditory neurons (*Pjvk*$^{-/-}$ mice).

(E and F) Examples of ABRs in *Pjvk*$^{-/-}$ and *Pjvk*$^{fl/fl}$Myo15-*cre*$^{+/-}$ mice: the latency of wave I is affected by controlled sound exposure in both mutant mice, and wave IV displays an additional increase in latency only in *Pjvk*$^{-/-}$ mice.

(G–I) Examples of EEBRs in *Pjvk*$^{+/+}$ (G), *Pjvk*$^{-/-}$ (H), and *Pjvk*$^{fl/fl}$Myo15-*cre*$^{+/-}$ (I) mice; EEBRs are affected by controlled electrical exposure only in *Pjvk*$^{-/-}$ mice.

(legend continued on next page)

We investigated possible changes in gene expression in the organ of Corti of P15 *Pjvk*$^{-/-}$ mice, by microarrays (see the Supplemental Experimental Procedures). Eighteen genes had expression levels at least 1.5-fold higher or lower in *Pjvk*$^{-/-}$ mice than in *Pjvk*$^{+/+}$ mice. Marked differences were observed for four genes involved in the redox balance—*CypA*, *Gpx2*, *c-Dct*, and *Mpv17*—encoding cyclophilin A, glutathione peroxidase 2, c-dopachrome tautomerase, and Mpv17, respectively (Table S1). All of these genes were downregulated in *Pjvk*$^{-/-}$ mice, a result confirmed by qRT-PCR (Figure S4A), and all encode antioxidant proteins, suggesting that *Pjvk*$^{-/-}$ mice have impaired antioxidant defenses (Table S1).

We thus assessed the level of oxidative stress in the cochlea of P21 *Pjvk*$^{-/-}$ mice, by determining the ratio of reduced to oxidized glutathione (GSH:GSSG). The GSSG content was about three times larger than in *Pjvk*$^{+/+}$ mice, whereas the GSH content was 23% smaller, resulting in a GSH:GSSG ratio in *Pjvk*$^{-/-}$ cochleas reduced by a factor of 3.4 (Figure 4A). Pejvakin deficiency thus results in cochlear oxidative stress.

We assessed lipid peroxidation by reactive oxygen species (ROS) in *Pjvk*$^{-/-}$ mice, by immunofluorescence-based detection of the by-product 4-hydroxy-2-nonenal (4-HNE). Strong immunoreactivity was observed in P60 *Pjvk*$^{-/-}$ hair cells and cochlear ganglion neurons (Figure S3B). Quantification of lipid peroxidation in microdissected organs of Corti from P30 *Pjvk*$^{-/-}$ and *Pjvk*$^{+/+}$ mice, showed a moderate, but statistically significant, increase of the malondialdehyde content in the absence of pejvakin (2.15 ± 0.14 μM in *Pjvk*$^{-/-}$ versus 1.84 ± 0.11 μM in *Pjvk*$^{+/+}$ mice; $p = 0.04$). Thus, pejvakin deficiency led to impaired antioxidant defenses in the cochlea, resulting in ROS-induced cell damage.

We then studied electrophysiological features of IHCs and OHCs in the mature cochlea of P19–P21 *Pjvk*$^{-/-}$ mice. In IHCs, the number of synaptic ribbons, Ca^{2+} currents, and synaptic exocytosis were unaffected (Figure S5A). We investigated whether *Pjvk*$^{-/-}$ mice display the main K^+ currents found in mature IHCs, specifically $I_{K,f}$, which plays a major part in IHC repolarization and is involved in the high temporal precision of action potentials in postsynaptic nerve fibers, $I_{K,s}$, and $I_{K,n}$ (Oliver et al., 2006). The $I_{K,f}$ current that flows through the large conductance voltage- and Ca^{2+}-activated potassium (BK) channels, a well-known target of ROS (Tang et al., 2004), was detected in only 4 out of 11 *Pjvk*$^{-/-}$ IHCs, and the mean number of spots immunolabeled for the BK α-subunit per IHC was much lower in *Pjvk*$^{-/-}$ mice (5.0 ± 1.4, n = 283 IHCs from seven mice) than in *Pjvk*$^{+/+}$ mice (13.9 ± 2.6, n = 204 IHCs from nine mice; t test, $p < 0.001$). By contrast, the $I_{K,s}$ and $I_{K,n}$ currents were not affected (Figures 4B and S5B). The electromotility of OHCs was moderately impaired in *Pjvk*$^{-/-}$ mice (Figure S5C). This contrasted with the total loss of DPOAE in a large majority of Pjvk$^{-/-}$ mice from P15 on, even at the highest possible stimulus level of 75 dB SPL. It thus pinpointed the existence of an additional defect, likely a mechanoelectrical transduction defect, the main determinant of DPOAEs at high stimulus levels (Avan et al., 2013). The decrease of the cochlear microphonic potential that reflects mechanoelectrical transduction currents through OHCs of the basal-most cochlear region, indeed corroborated the DPOAE measurements: this potential, recorded for a 5-kHz sound stimulus at 95 dB SPL, was always larger than 10 μV in *Pjvk*$^{+/+}$ mice (n = 8), but fell between 5 and 3 μV in the P21 *Pjvk*$^{-/-}$ mice with residual DPOAEs (n = 2), and below 1 μV, in the *Pjvk*$^{-/-}$ mice without persisting DPOAEs (n = 6). Taken together, oxidative stress in the *Pjvk*$^{-/-}$ cochlea impacts various electrophysiological properties of the hair cells, particularly mechanoelectrical transduction and K^+ current through BK channels.

Mitochondrial defects are a common cause of ROS overproduction. However, we did not find evidence that mitochondria were damaged, as vulnerability of the mitochondrial membrane potential, $\Delta\psi_m$, to the uncoupler carbonyl cyanide 4-(trifluoromethoxy)phenylhydrazone (FCCP) in the organ of Corti and cochlear ganglion was similar in P17-P30 *Pjvk*$^{-/-}$ and *Pjvk*$^{+/+}$ mice, and analysis of *Pjvk*$^{-/-}$ hair cells by transmission electron microscopy (TEM) revealed no mitochondrial abnormalities (Figure S5D; data not shown).

Pejvakin Is a Peroxisome-Associated Protein

By using *Pjvk*$^{-/-}$ cochlea as control, we found that neither the commercially available antibodies nor our initial polyclonal antibody (Delmaghani et al., 2006) specifically recognized pejvakin (data not shown). Given the limited divergence of the pejvakin amino-acid sequence among vertebrates, we tried to elicit an immune response in *Pjvk*$^{-/-}$ mice (see the Experimental Procedures). The monoclonal antibody obtained, Pjvk-G21, labeled peroxisomes stained by peroxisome membrane protein 70 (PMP70) antibodies in transfected HeLa cells expressing pejvakin (Figure S6A) and in the human HepG2 hepatoblastoma cell line, which is particularly rich in this organelle (Figure 5A). The specificity of the Pjvk-G21 antibody was demonstrated by the immunolabeling of peroxisomes in the hair cells of *Pjvk*$^{+/+}$, but not of *Pjvk*$^{-/-}$ and *Pjvk*$^{fl/fl}$Myo15-*cre*$^{+/-}$ mice (Figures 5B and S6B).

Prediction programs failed to detect the PTS1 or PTS2 motifs in the pejvakin sequence (Mizuno et al., 2008), the targeting signals for the importation of peroxisomal matrix proteins into the organelle (Smith and Aitchison, 2013), suggesting that pejvakin is a peroxisomal membrane or membrane-associated protein.

Structural Abnormalities of Peroxisomes in the Hair Cells of *Pjvk*$^{-/-}$ Mice

We investigated the distribution and morphology of peroxisomes by TEM. Peroxisomes were identified on the basis of catalase activity detection using 3,3′-diaminobenzidine as substrate. We focused on OHCs, the first to display a dysfunction in *Pjvk*$^{-/-}$ mice. On P30, but not on P15, both the distribution and shape of peroxisomes differed between *Pjvk*$^{-/-}$ and *Pjvk*$^{+/+}$ mice (Figure 5E). In *Pjvk*$^{+/+}$ OHCs, the peroxisomes were restricted to an area immediately below the cuticular plate. In *Pjvk*$^{-/-}$ mice,

(J–L) Neuronal function rescue in *Pjvk*$^{-/-}$ mice by transduction with AAV8-Pjvk: effects on ABR interwave I-IV latency (J), on EEBR wave E IV amplitude and its hypervulnerability to electrical stimulation (K), and on EEBR interwave E II-E IV latency (one example is shown in L, to be compared with H). Vertical arrows indicate the positions of waves I and IV on ABR traces and of waves E II and E IV on EEBR traces. ns, not significant; ***$p < 0.001$. Error bars represent the SD. See also Figures S1 and S2A.

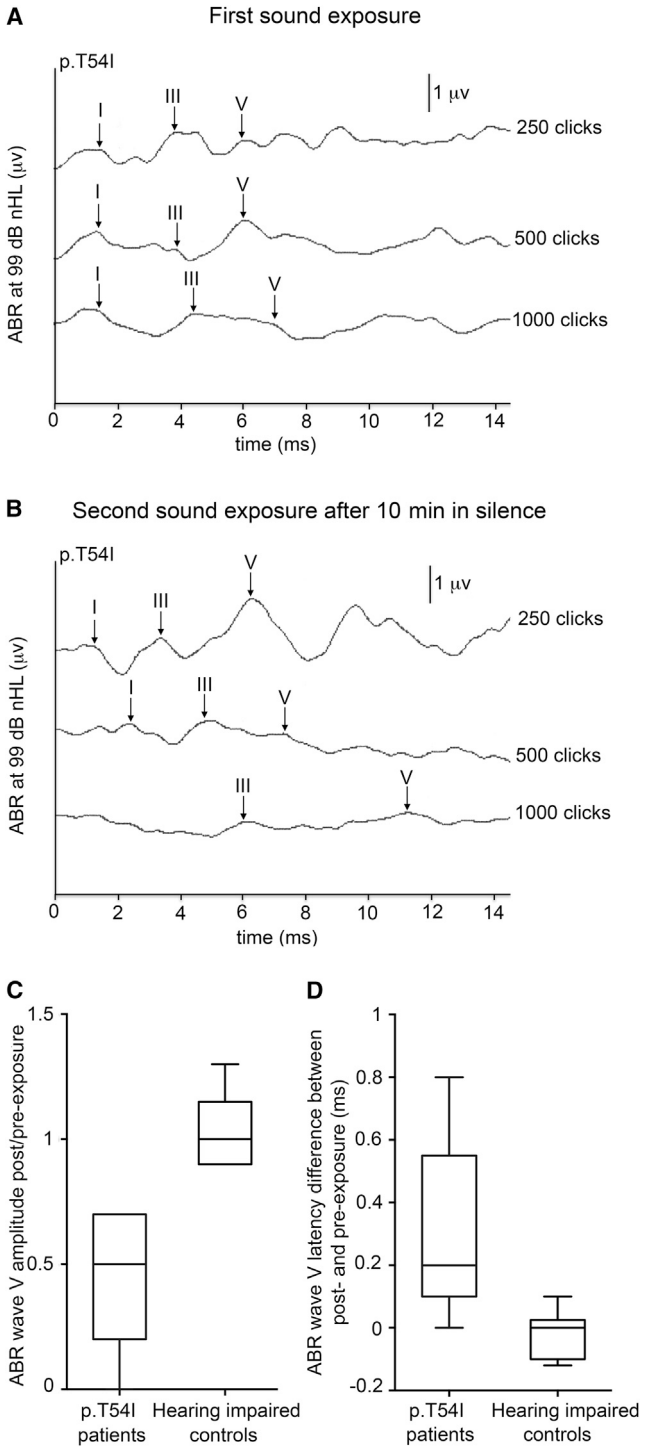

Figure 3. Hypervulnerability to Sound in DFNB59 Patients

(A) ABR waves I, III, and V (vertical arrows) in one ear of a patient carrying the *PJVK* p.T54I mutation, in response to 250, 500, and 1000 impulse stimuli (clicks) at 99 dB nHL.

(B) Repeated ABRs after 10 min of silence, with an even larger vulnerability of waves I, III, and V.

(C and D) Distributions of the amplitude (C) and latency (D) of ABR wave V in the tested sample of p.T54I patients (n = 8 ears), and in a control group of patients (n = 13) with cochlear hearing impairment and matched ABR thresholds, before and after exposure to clicks #250 to #1000. Boxes extend from the 25th to the 75th percentile. Horizontal bars and vertical bars indicate median values and extremes, respectively. Unlike the unaffected controls, all p.T54I patients displayed markedly decreased amplitudes and increased latencies.

the peroxisomes located just below the cuticular plate were slightly larger than those in $Pjvk^{+/+}$ mice. Strikingly, irregular catalase-containing structures, some of which were juxtaposed, were present in the perinuclear region, in the immediate vicinity of the nuclear membrane of all $Pjvk^{-/-}$ OHCs, but not of $Pjvk^{+/+}$ OHCs (Figure 5E). The lack of pejvakin thus results in peroxisome abnormalities in OHCs after the onset of hearing.

Pejvakin Is Involved in Oxidative Stress-Induced Peroxisome Proliferation

In HepG2 cells, protrusions emerging from some peroxisomes, the first step of peroxisome biogenesis from pre-existing peroxisomes, were immunoreactive for pejvakin. String-of-beads structures corresponding to elongated and constricted peroxisomes, preceding final fission (Smith and Aitchison, 2013), were also pejvakin-immunoreactive, suggesting a role for this protein in peroxisome proliferation (Figure S6C). Peroxisomes actively contribute to cellular redox balance, by producing and scavenging/degrading H_2O_2 through a broad spectrum of oxidases and peroxidases (especially catalase), respectively (Schrader and Fahimi, 2006). Because $Pjvk^{-/-}$ mice displayed features of marked oxidative stress in the cochlea, we investigated the possible role of pejvakin in peroxisome proliferation in response to oxidative stress induced by H_2O_2 (Lopez-Huertas et al., 2000). Embryonic fibroblasts derived from $Pjvk^{+/+}$ and $Pjvk^{-/-}$ mice were exposed to H_2O_2 (see the Supplemental Experimental Procedures). In unexposed cells, the number of peroxisomes was similar between the two genotypes (t test, $p = 0.82$). After H_2O_2 treatment, it increased by 46% in $Pjvk^{+/+}$ fibroblasts ($p = 0.004$), but remained unchanged in $Pjvk^{-/-}$ fibroblasts ($p = 0.83$), resulting in a statistically significant difference between the two genotypes ($p < 0.001$) (Figures 5C and S7A).

We then asked whether mutations reported in DFNB59 patients also affect peroxisome proliferation. We assessed the number of peroxisomes in transfected HeLa cells producing EGFP alone, EGFP and murine pejvakin, or EGFP and one of the mutated forms of murine pejvakin carrying the mutations responsible for DFNB59 (p.T54I, p.R183W, p.C343S, or p.V330Lfs*7). Cells producing the non-mutated pejvakin had larger numbers of peroxisomes than cells producing EGFP alone, whereas cells producing any of the mutated forms of pejvakin (mutPjvk-IRES-EGFP) had smaller peroxisome numbers. In addition, many of these cells contained enlarged peroxisomes, a feature typical of peroxisome proliferation disorders (Ebberink et al., 2012) (Figure 5D and S7B). Together, these results strongly suggest that pejvakin is directly involved in the production of new peroxisomes from pre-existing peroxisomes.

Upregulation of *Pjvk* Cochlear Transcription and Peroxisome Proliferation in Response to Sound

We then asked whether pejvakin is involved in the physiological response to sound. We first assessed the transcription of *Pjvk*

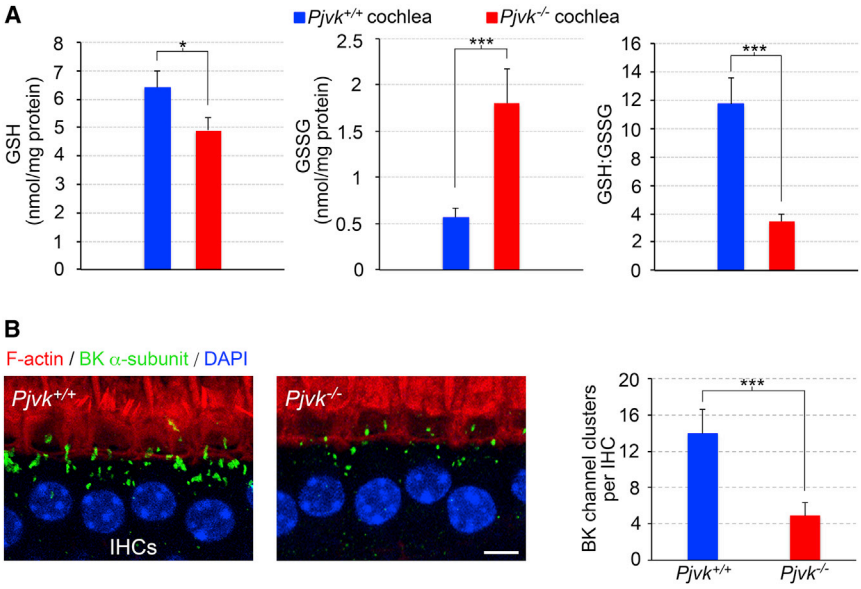

Figure 4. Increased Oxidative Stress and ROS-Induced Cell Damage in the *Pjvk*$^{-/-}$ Cochlea

(A) Reduced glutathione (GSH) (left bar chart), oxidized-glutathione (GSSG) (middle bar chart) contents, and GSH:GSSG ratio (right bar chart) in P21 *Pjvk*$^{-/-}$ versus *Pjvk*$^{+/+}$ cochlea. Error bars represent the SEM of three independent experiments. See also Figure S3.

(B) Marked decrease in the BK α-subunit immunolabeling in *Pjvk*$^{-/-}$ IHCs. Left: P20 *Pjvk*$^{+/+}$ and *Pjvk*$^{-/-}$ IHCs. Scale bar is 5 μm. Right: quantitative analysis of BK channel clusters. Error bars represent the SD. See also Figure S5B. *p < 0.05, ***p < 0.001.

See also Figures S3 and S5.

and of *CypA*, *Gpx2*, *c-Dct*, and *Mpv17*, which were downregulated in *Pjvk*$^{-/-}$ mice, in microdissected organs of Corti from P21 wild-type mice, with or without prior sound stimulation (5–20 kHz, 105 dB SPL for 1 hr; see the Supplemental Experimental Procedures). Transcript levels were analyzed by qRT-PCR at various times (1, 3, 6, and 18 hr) after sound exposure (Figure 6A). *Pjvk* transcript levels had increased by factors of 1.9 ± 0.1 and 3.5 ± 0.7, mean ± SEM, after 1 and 6 hr, respectively. *CypA*, *c-Dct*, and *Mpv17* were also upregulated after 6 hr (by factors of 6.6 ± 1.2, 4.3 ± 0.6, and 1.5 ± 0.1, respectively), as were *c-Fos* and *Hsp70*, used as a positive control, but not *Gpx2*. Thus, noise exposure leads to an upregulation of the transcription of *Pjvk* and of genes downregulated in *Pjvk*$^{-/-}$ mice, and this effect is dependent on acoustic energy level of the stimulation (Figure S4B).

This result predicted that sound exposure would lead to peroxisome proliferation in the auditory system of wild-type mice. 6 hr after exposure (5–20 kHz, 105 dB SPL for 1 hr), the numbers of peroxisomes were unchanged (34.5 ± 0.8 and 35.9 ± 1.0, mean ± SEM, per IHC from unexposed and sound-exposed mice, respectively, n = 75 cells from six mice; t test, p = 0.25). However, at 48 hr, they had markedly increased, by a factor of 2.3, in both IHCs and OHCs (84.7 ± 5.0 per IHC and 16.5 ± 1.0 per OHC, n = 90 cells and n = 150 cells from six mice, respectively) compared to unexposed mice (36.8 ± 3.0 per IHC and 7.3 ± 0.4 per OHC, n = 90 cells and n = 150 cells from six mice, respectively; t test, p < 0.0001 for both comparisons). The number of peroxisomes had also increased, by 35%, in the dendrites of primary auditory neurons (1.7 ± 0.1 and 2.3 ± 0.2 peroxisomes per micrometer of neurite length, n = 40 neurites from five unexposed and five sound-exposed *Pjvk*$^{+/+}$ mice, respectively; t test, p = 0.003) (Figure 6B).

Therapeutic Approaches in *Pjvk*$^{-/-}$ Mice

Based on these results, we tested whether the classical antioxidant drug N-acetyl cysteine (NAC) (either alone or associated with α-lipoic acid and α-tocopherol; see the Supplemental Experimental Procedures) administered to *Pjvk*$^{-/-}$ pups could improve their hearing. The ABR thresholds of P21 NAC-treated *Pjvk*$^{-/-}$ pups (n = 21) were about 10 dB lower than those of untreated *Pjvk*$^{-/-}$ pups (n = 24) for all frequencies tested (t test, p < 0.001 for all comparisons) (Figure 7A). The amplitude of the ABR wave I elicited at 105 dB SPL (4.35 ± 1.16 μV, n = 21) was the same as that of *Pjvk*$^{+/+}$ mice (4.36 ± 1.15 μV, n = 18; t test, p = 0.97) and greater than that of untreated *Pjvk*$^{-/-}$ mice (1.88 ± 1.07 μV, n = 24; t test, p < 0.001) (Figure 7B). EEBRs were more resistant to the high-rate electrical stimulation in treated than in untreated mutant mice (Figure 7C). Conversely, NAC had no beneficial effect on OHCs (data not shown). The association of NAC with α-lipoic acid and α-tocopherol did not perform any better (data not shown).

Full recovery of the neuronal phenotype was achieved by the intracochlear injection of AAV8-Pjvk (see above). As hair cells are not transduced by AAV8, we investigated whether AAV2/8, which transduces hair cells only (Figure S2B), could rescue the *Pjvk*$^{-/-}$ hair-cell phenotype. The auditory function of *Pjvk*$^{-/-}$ mice (n = 7, four pups per cage in every experiment) receiving intracochlear injections of AAV2/8-Pjvk-IRES-EGFP on P3 was assessed on P21, and the percentage of transduced IHCs and OHCs was evaluated in each injected and contralateral (not injected) cochlea, on the basis of EGFP fluorescence. Improvements in ABR thresholds of 20 to 30 dB SPL with respect to untreated mice were observed for frequencies between 10 and 20 kHz (t test, p < 0.001 for all comparisons; Figure 7D). Upon injection of AAV2/8-EGFP, DPOAEs, ABR thresholds, and ABR wave I amplitude and latency were similar to those of untreated *Pjvk*$^{-/-}$ mice (data not shown). A partial reversion of the OHC dysfunction was obtained, with detectable DPOAEs in pejvakin cDNA-treated cochleas (threshold 54.0 ± 10.7 dB), but not in contralateral, untreated cochleas (Figure 7E). DPOAE thresholds were linearly correlated (r^2 = 0.74, p < 0.001) with the number of EGFP-tagged OHCs (Figure 7F), suggesting that the normalization of DPOAE thresholds may be possible if all OHCs could be transduced. The latency of the ABR wave I in response to a 105 dB SPL stimulation decreased significantly (1.38 ± 0.11 ms for the treated ears; n = 6, versus 1.53 ± 0.10 ms

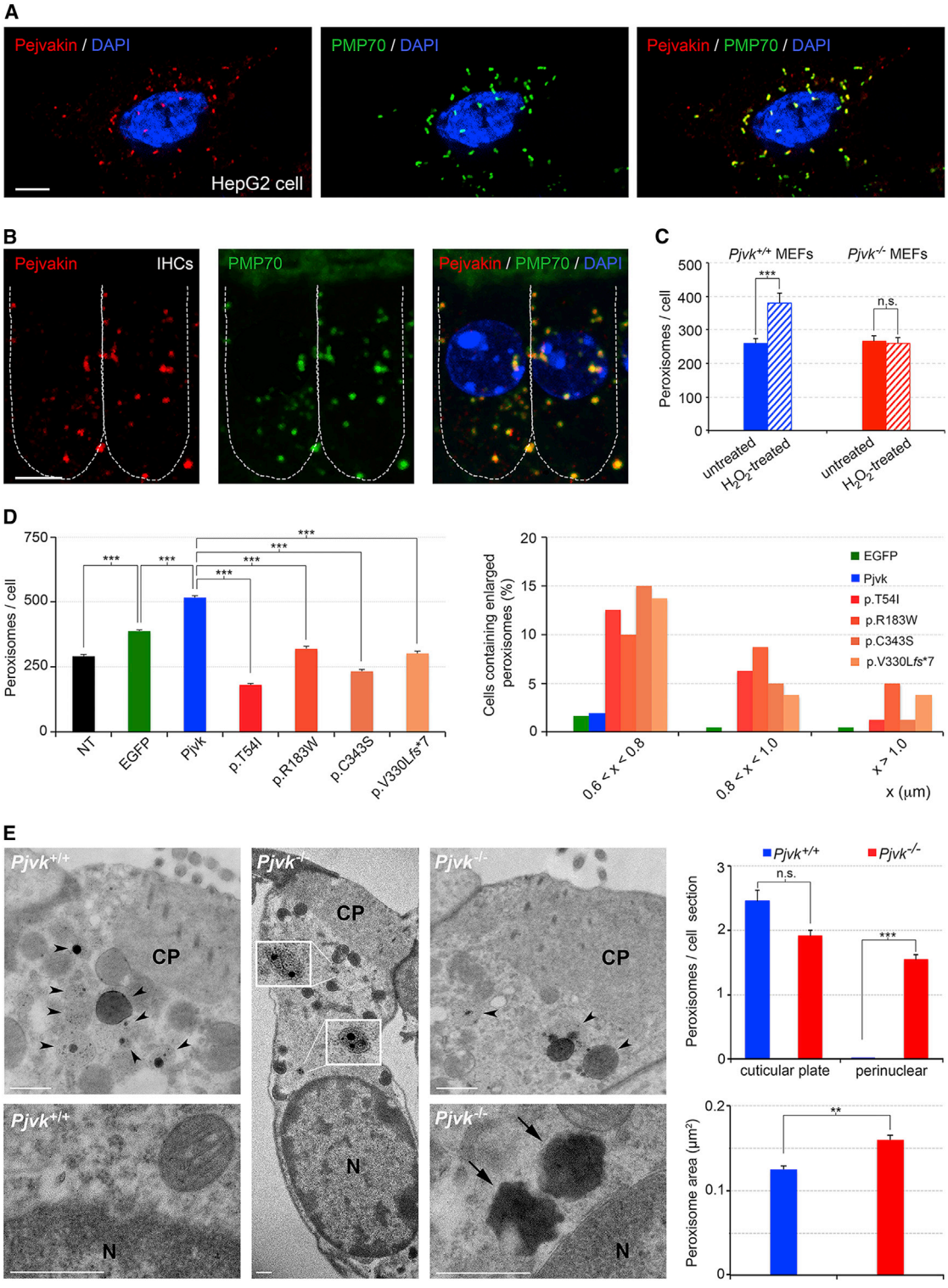

Figure 5. Pejvakin Is a Peroxisome-Associated Protein Involved in the Oxidative Stress-Induced Peroxisomal Proliferation

(A and B) Immunolabeling of PMP70 and endogenous pejvakin in a HepG2 cell (A) and in two P20 *Pjvk*$^{+/+}$ IHCs (B). See also Figure S6B.

(C) Number of peroxisomes in *Pjvk*$^{+/+}$ and *Pjvk*$^{-/-}$ mouse embryonic fibroblasts (MEFs) subjected to 0.5 mM H_2O_2 versus untreated MEFs (n = 30 cells for each condition). See also Figure S7A.

(D) Untransfected HeLa cells (NT) and transfected cells producing either EGFP alone or EGFP, together with the wild-type pejvakin (Pjvk) or a mutated Pjvk (p.T54I, p.R183W, p.C343S, or p.V330L*fs**7). Left panel: bar chart showing the numbers of peroxisome per cell 48 hr after transfection. There were on average

(legend continued on next page)

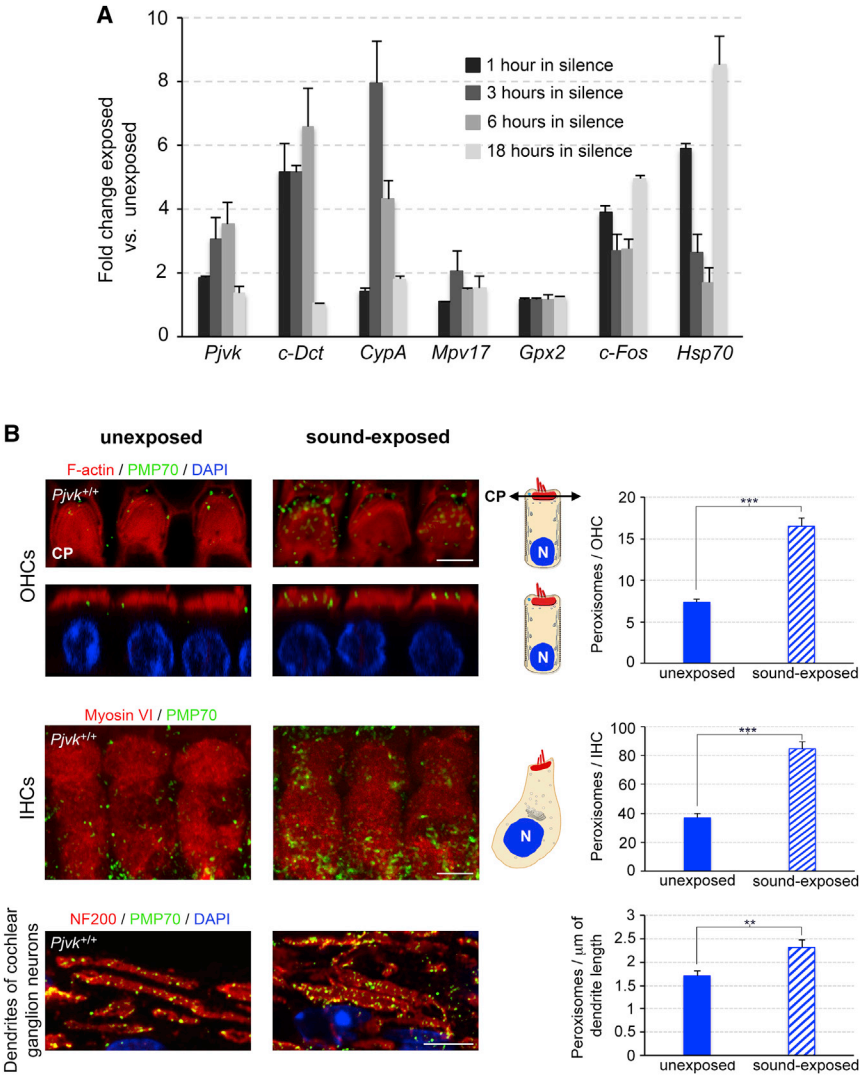

Figure 6. Effect of Exposure to Loud Sounds on the Cochlear Expression of *Pjvk* and the Number of Peroxisomes in Cochlear Hair Cells and Ganglion Neurons

(A) *Pjvk*, *c-Dct*, *CypA*, *Mpv17*, and *Gpx2* transcript levels assessed by qRT-PCR in P21 $Pjvk^{+/+}$ organ of Corti 1, 3, 6, and 18 hr after sound exposure (5–20 kHz, 105 dB SPL for 1 hr). The levels of *c-Fos* and *Hsp70* transcripts were used as positive controls. See also Figure S4B.

(B) Peroxisome proliferation in P21 $Pjvk^{+/+}$ hair cells and cochlear ganglion neurons after sound exposure (same conditions as in A). Peroxisomes were counted 48 hr after sound exposure. OHCs, IHCs, and neuronal processes stained for F-actin, myosin VI, and neurofilament protein NF200, respectively. In OHCs and IHCs, the peroxisomes are located below the CP and throughout the cytoplasm, respectively. For OHCs, both a lateral view and a transverse optical section at the level of CP (scheme on the right) are shown. The number of peroxisomes was increased in OHCs, IHCs, and dendrites after sound exposure. N, cell nucleus. ***p < 0.001. Error bars represent the SEM. Scale bars are 5 µm.

See also Figure S4 and Table S1.

for the contralateral, untreated ears; paired t test, p = 0.03) (Figure 7G), and its amplitude increased into the normal range (7.34 ± 0.80 µV versus 2.93 ± 0.92 µV; paired t test, p < 0.001) (Figure 7H), in relation to the number of EGFP-tagged IHCs (r^2 = 0.89 for wave I amplitude, p < 0.001; Figure 7I). No correction of the interwave I-IV latency was observed, as expected (data not shown).

Finally, we investigated the effect of the transduction of $Pjvk^{-/-}$ IHCs by AAV2/8-Pjvk-IRES-EGFP on their peroxisomes. Before sound exposure, the numbers of peroxisomes in IHCs of P21 $Pjvk^{-/-}$ and AAV2/8-Pjvk-IRES-EGFP-injected $Pjvk^{-/-}$ mice did not differ from that of $Pjvk^{+/+}$ mice (30.5 ± 1.9, 32.3 ± 2.1, and 36.8 ± 3.0 peroxisomes, mean ± SEM per IHC, n = 60 cells from four $Pjvk^{-/-}$ and four AAV2/8-Pjvk $Pjvk^{-/-}$ mice, and n = 90 cells from six $Pjvk^{+/+}$ mice, respectively; t test, p = 0.11 and p = 0.30, respectively). By contrast, 48 hr after sound exposure (5–20 kHz) at 105 dB SPL for 1 hr, the number of peroxisomes had decreased by 63% in $Pjvk^{-/-}$ IHCs (30.5 ± 1.9 and 11.2 ± 1.3 peroxisomes per IHC, n = 75 cells from five unexposed and five sound-exposed $Pjvk^{-/-}$ mice, respectively; t test, p < 0.0001), and enlarged PMP70-labeled structures were present close to the nucleus (Figure 7J). In response to the same sound but of a lower intensity, i.e., 97 dB SPL for 1 hr, the number of peroxisomes was unchanged in $Pjvk^{-/-}$ IHCs (30.5 ± 1.9 and 34.6 ± 2.3 peroxisomes per IHC, n = 60 cells from four unexposed and four sound-exposed $Pjvk^{-/-}$ mice,

33% more peroxisomes in cells producing both EGFP and Pjvk (n = 200) than in cells producing EGFP alone (n = 150). Right panel: for every range of enlarged peroxisome size, x (0.6–0.8 µm, 0.8–1.0 µm, and >1.0 µm), in two perpendicular directions, the proportion of cells containing at least one peroxisome. See also Figure S7B.

(E) Abnormalities in shape and distribution of peroxisomes in mature $Pjvk^{-/-}$ OHCs detected by TEM (P30 $Pjvk^{-/-}$ [middle and right] and $Pjvk^{+/+}$ [left] OHCs). Insets [middle panel]: enlarged views of individual peroxisomes. In $Pjvk^{+/+}$ OHCs, peroxisomes are grouped just under the cuticular plate (CP) (arrowheads), with none detected in the perinuclear region (n = 33 sections, upper bar chart). In $Pjvk^{-/-}$ OHCs, some peroxisomes remain under the CP (arrowheads), but catalase-containing structures, misshapen peroxisomes (arrows), are detected in the perinuclear region (n = 24 sections, upper bar chart). Peroxisomes located under the CP are larger in $Pjvk^{-/-}$ OHCs (n = 92 peroxisomes) than in $Pjvk^{+/+}$ OHCs (n = 89 peroxisomes) (lower bar chart). N, cell nucleus. **p < 0.01, ***p < 0.001. Error bars represent the SEM. Scale bars are 5 µm in (A) and (B) and 0.5 µm in (E).

See also Figures S6 and S7.

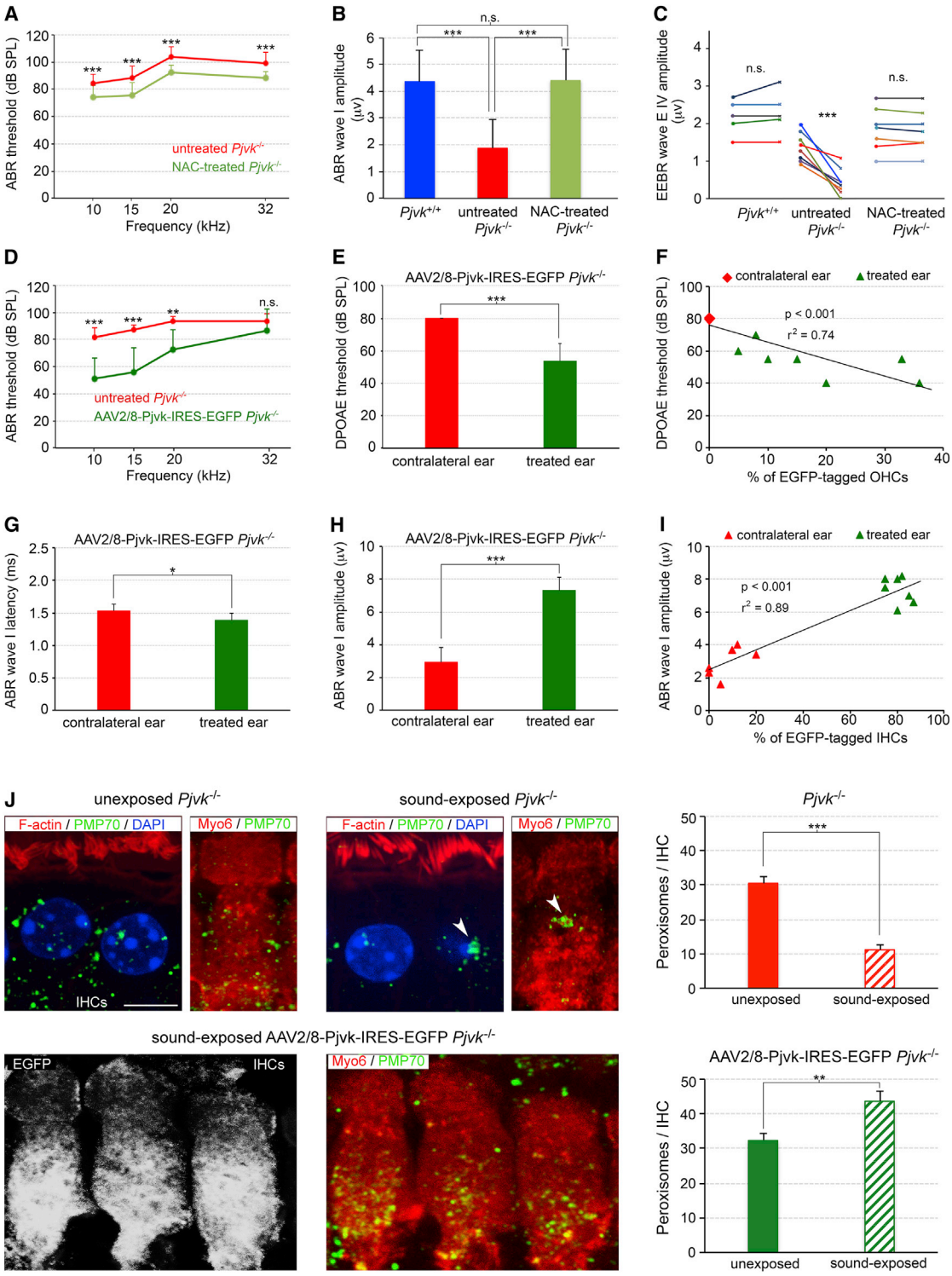

Figure 7. Therapeutic Approaches in *Pjvk*$^{-/-}$ Mice

(A–C) Effect of N-acetyl cysteine (NAC) on auditory function in *Pjvk*$^{-/-}$ mice. (A) ABR thresholds in untreated versus NAC-treated P21 *Pjvk*$^{-/-}$ mice. (B) ABR wave I amplitude for 10 kHz tone bursts in *Pjvk*$^{+/+}$ and untreated *Pjvk*$^{-/-}$ versus NAC-treated *Pjvk*$^{-/-}$ mice at P21. (C) EEBR wave E IV amplitude before (dots) and after (crosses) controlled electrical stimulation of the cochlear nerve at 200 impulses/s for 1 min in *Pjvk*$^{+/+}$, untreated *Pjvk*$^{-/-}$, and NAC-treated *Pjvk*$^{-/-}$ mice.

(D–I) Effect of AAV2/8-Pjvk-IRES-EGFP transferred into the cochlear hair cells on the auditory function of *Pjvk*$^{-/-}$ mice. See also Figure S2B. (D) ABR thresholds at 10, 15, and 20 kHz in AAV2/8-Pjvk-IRES-EGFP-treated versus untreated *Pjvk*$^{-/-}$ mice. (E and H) DPOAE threshold (E) and ABR wave I amplitude (H) at 10 kHz in

(legend continued on next page)

respectively; t test, p = 0.17), and no enlarged PMP70-stained structures were detected (data not shown). The absence of pejvakin thus resulted in defective sound-induced peroxisomal proliferation (both at 105 dB SPL and 97 dB SPL) and, even, in peroxisome degeneration (at 105 dB SPL) in IHCs. In *Pjvk*$^{-/-}$ mice injected with AAV2/8-Pjvk-IRES-EGFP on P3 and exposed to 105 dB SPL for 1 hr on P21, enlarged PMP70-labeled structures were no longer detected in transduced IHCs, and the number of peroxisomes increased by 35% (32.3 ± 2.1 and 43.7 ± 3.0 peroxisomes per IHC, n = 60 cells from unexposed and exposed transduced *Pjvk*$^{-/-}$ IHCs, respectively; t test, p = 0.002) (Figure 7J). We conclude that pejvakin re-expression fully protects *Pjvk*$^{-/-}$ IHCs from the degenerescence of peroxisomes and partially restores their impaired adaptive proliferation.

DISCUSSION

Noise-induced hearing loss (NIHL) is the second most common form of sensorineural hearing impairment after presbycusis in the United States (Dobie, 2008). Here, we describe a genetic form of NIHL, by showing that pejvakin deficiency in mice and DFNB59 patients leads to hypervulnerability to sound, due to a peroxisomal deficiency. To our knowledge, a peroxisomal cause of an isolated (non-syndromic) form of inherited deafness has not been reported yet. The peroxisome emerges as a key organelle in the redox homeostasis of the auditory system, for coping with the overproduction of ROS induced by high levels of acoustic energy.

Acoustic energy is the main determinant of NIHL. The $L_{EX,8\ hr}$ (for level of exposure over an 8-hr workshift) index has been defined such that an $L_{EX,8\ hr}$ of X dB delivers the same energy as a stable sound of X dB played over a period of 8 hr. Chronic occupational exposures to less than 85 dB (or 80 dB, depending on the country) are deemed safe. In *Pjvk*$^{-/-}$ mice, a single exposure to 63 dB $L_{EX,8\ hr}$ increased hearing thresholds by 30 dB, with full recovery occurring after about 2 weeks. By contrast, a ten times more energetic exposure to a $L_{EX,8\ hr}$ of 73 dB in wild-type mice of the same strain produces only an 18 dB shift in threshold, with a recovery time of 12 hr (Housley et al., 2013). This hypersensitivity of *Pjvk*$^{-/-}$ mice to noise suggests that the $L_{EX,8\ hr}$ of about 83 dB for a cage of ten pups is sufficient to account for permanent hearing loss in these *Pjvk*$^{-/-}$ pups, while some of those housed in small numbers in quiet rooms can display near-normal hearing thresholds (see Figure 1C). Likewise, the auditory function of DFNB59 patients was transiently affected by a 57 dB $L_{EX,8\ hr}$ exposure, routinely used in ABR tests.

NIHL involves the excessive production of ROS, overwhelming the antioxidant defense system and causing irreversible oxidative damage to DNA, proteins, and lipids within the cell (Henderson et al., 2006). Noise-induced oxidative stress results in the production of H_2O_2 and other ROS as by-products, thought to derive from the intense solicitation of mitochondrial activity, and several mouse mutants with mitochondrial defects are prone to NIHL (Ohlemiller et al., 1999; Brown et al., 2014). Our studies of pejvakin-deficient mouse mutants and rescue experiments targeting the hair cells and auditory neurons unambiguously show that IHCs, OHCs, primary auditory neurons, and neurons of the cochlear nucleus are hypervulnerable to sound in the absence of pejvakin, which is consistent with previous results showing that hair cells and neurons of the auditory system are targets of NIHL (Wang et al., 2002; Kujawa and Liberman, 2009; Imig and Durham, 2005). However, our study goes one step further by implicating a possible common mechanism: peroxisomal failure, the importance of which is demonstrated by the impairment of the redox homeostasis caused by pejvakin deficiency. It also reveals a major cause of the unusually high level of phenotypic variability observed in pejvakin-deficient mice and humans: the difference in sound exposure and the inability of the peroxisomes to cope with the resultant activity-dependent oxidative stress in the absence of pejvakin. Incidentally, this can account for the apparent paradox that mice carrying the R183W mutation in pejvakin displayed a much more severe neural pathway defect than the *Pjvk*$^{-/-}$ mice (Delmaghani et al., 2006). Due to the preservation of hair cell functions, the auditory neurons of R183W mutant mice should be strongly stimulated, whereas the early permanent damage to cochlear hair cells in *Pjvk*$^{-/-}$ mice acts as a protective "muffler" of the neuronal pathway.

In mammals, the number and metabolic functions of peroxisomes differ between cell types. However, all cell types are able to adapt rapidly to modifications in physiological conditions by changing the number, shape, size, and molecular content of peroxisomes, resulting in considerable functional plasticity of these organelles (Schrader et al., 2012; Smith and Aitchison, 2013). Our experiments on *Pjvk*$^{-/-}$ and *Pjvk*$^{+/+}$ mouse embryonic fibroblasts stressed with H_2O_2 showed that pejvakin is critically involved in the oxidative stress-induced proliferation of peroxisomes through growth and fission of pre-existing peroxisomes. The molecular machinery underlying this adaptive process is still poorly understood beyond the involvement of Pex11α (Li et al., 2002). Of note, the absence of pejvakin only affects the proliferation of peroxisomes from pre-existing peroxisomes, but not the constitutive biogenesis of this organelle. Accordingly, structural abnormalities of peroxisomes in *Pjvk*$^{-/-}$ mice became apparent only after hearing onset, in the context of the oxidative stress produced by noise exposure. By contrast, the *PEX* gene defects causing Zellweger syndrome spectrum (ZSS) disorders (Waterham and Ebberink, 2012) and rhizomelic chondrodysplasia punctata affect the constitutive biogenesis of peroxisomes. Hearing impairment in ZSS disorders involves a severe impairment of neuronal conduction and has been attributed to defects in the synthesis of two essential myelin sheath components—plasmalogens and docosahexaenoic acid—which is critically dependent on peroxisomes. Our results suggest that ZSS also

treated versus untreated contralateral ears. (G) ABR wave I latency in treated versus untreated contralateral ears. (F) Correlation between DPOAE thresholds and the proportion of EGFP-tagged (i.e., transduced) OHCs. Six untreated ears have no recordable DPOAE (threshold arbitrarily set at 80 dB SPL; red diamond). (I) Correlation between ABR wave I amplitude at 10 kHz, 105 dB SPL, and the percentage of transduced IHCs (EGFP tagged).

(J) Effect of AAV2/8-Pjvk-IRES-EGFP on the peroxisomes in *Pjvk*$^{-/-}$ IHCs. Upper and lower panels show and quantify (bar charts) the peroxisomes in untreated mice 48 hr after sound exposure (5–20 kHz, 105 dB SPL for 1 hr) (peroxisome abnormalities are indicated by arrowheads). Error bars represent the SD in (A–I) and the SEM in (J). ns, not significant; *p < 0.05, **p < 0.01, ***p < 0.001.

includes a defective redox balance in the hair cells and neurons of the auditory system.

In the context of noise exposure, the upregulation of *Pjvk* transcription in the cochlea and the subsequent peroxisome proliferation in the hair cells and auditory neurons of wild-type mice suggest that pejvakin-dependent peroxisome proliferation in the auditory system is part of the physiological response to high levels of acoustic energy that result in increased amounts of ROS. This and the marked oxidative stress detected in the $Pjvk^{-/-}$ cochlea imply that the proliferation of peroxisomes plays an antioxidant role, similar to that reported in other cell types (Santos et al., 2005; Diano et al., 2011). The rapid elevation of the hearing threshold in $Pjvk^{-/-}$ mice in response to low-energy sounds and the increase in interwave I-IV latency observed in DFNB59 patients within a few seconds are consistent with an activity-dependent H_2O_2 production that, due to impaired cellular redox homeostasis, results in concentrations of H_2O_2 high enough to impact on the activity of various target proteins including ion channels and transporters (Rice, 2011). The worsening of hearing sensitivity, 2 days later, in the mutant mice lacking pejvakin, exacerbated by putting back the mice in a noisy environment, fits the picture of the absence of sound-induced biogenesis of peroxisomes (with their degeneration occurring in a high acoustic energy environment). We thus conclude that the hypervulnerability of $Pjvk^{-/-}$ mice and DFNB59 patients to sound does not result simply from an exacerbation, by sound, of a pre-existing redox-balance defect, but is the consequence of impaired adaptive proliferation of peroxisomes in the absence of pejvakin. Both defective peroxisome proliferation in IHCs of $Pjvk^{-/-}$ mice in response to sound exposure and its partial recovery by pejvakin cDNA transfer support this conclusion. A full recovery of the adaptive peroxisome proliferation produced by sound exposure may require higher concentrations of pejvakin or the sound-induced modulation of *Pjvk* transcription (see Figure 6A), which was missing in our rescue experiments (pejvakin cDNA expression being driven by a constitutive promoter).

In patients with hearing impairment, the amplification of sound by hearing aids or direct electrical stimulation of the auditory nerve by a cochlear implant delivers a stimulus with an energy level similar to that shown here to worsen the hearing impairment of $Pjvk^{-/-}$ mice within 1 min of sound exposure. Therefore, in cases of peroxisomal deficiency, as in DFNB59, specific protection against redox homeostasis failure is essential. Patients with such conditions should avoid noisy environments and a beneficial effect of hearing devices should require an antioxidant protection. N-acetyl cysteine was the only antioxidant drug tested here to display some, albeit limited, efficacy. By contrast, AAV-mediated gene therapy could potentially provide full protection. Finally, deciphering the sound-stress-induced protective signaling pathway involving pejvakin might lead to the discovery of therapeutic agents for NIHL.

EXPERIMENTAL PROCEDURES

Audiological Studies in Mice

Auditory tests were performed in an anechoic room, on anesthetized animals whose core temperatures were maintained at 37°C (see the Supplemental Experimental Procedures).

Audiological Tests in Patients

Informed consent was obtained from all the subjects included in the study. Pure-tone audiometry was performed with air- and bone-transmitted tones. Hearing impairment was assessed objectively, by measuring ABRs and transient-evoked otoacoustic emissions (TEOAEs). The nonlinear TEOAE recording procedure was used (derived from the ILO88 system), making it possible to extract TEOAEs from linear reflection artifacts from the middle ear, and to evaluate background noise. TEOAE responses were analyzed in 1-kHz-wide bands centered on 1, 2, 3 and 4 kHz.

Generation of an Anti-pejvakin Monoclonal Antibody

The 3′ end of the coding sequence of the Pjvk cDNA (NCBI:NM_001080711.2) was inserted into a pGST-parallel-2 vector (derived from pGEX-4T-1; Amersham). The resultant construct, encoding the C-terminal region of pejvakin (residues 290–352; RefSeq:NP_001074180.1) fused to an N-terminal glutathione S-transferase tag, was introduced into *Escherichia coli* BL21-Gold (DE3)-competent cells (Stratagene). The pejvakin protein fragment was purified on a glutathione-Sepharose 4B column, then subjected to size-exclusion chromatography and used as the antigen for immunization. Antibodies were produced by immunizing $Pjvk^{-/-}$ mice. An immunoglobulin G monoclonal antibody (K_D of 6×10^{-8} M), Pjvk-G21, was selected by ELISA on immunogen-coated plates.

Statistical Analyses

Quantitative data are presented as mean ± SD, unless otherwise mentioned. Statistical analyses were performed using GraphPad. Data were analyzed by paired or unpaired Student's t tests and, for multiple comparisons, either by one-way or two-way ANOVA or by t tests with the Bonferroni correction. Statistical significance of the differences observed between groups is defined as $p < 0.05$.

ACCESSION NUMBER

The accession number for the transcriptomic data reported in this paper is deposited in GEO:GSE72722.

SUPPLEMENTAL INFORMATION

Supplemental Information includes Supplemental Experimental Procedures, seven figures, and one table and can be found with this article online at http://dx.doi.org/10.1016/j.cell.2015.10.023.

AUTHOR CONTRIBUTIONS

C.P. and P.A. designed the study. S. Delmaghani designed and performed most of the experiments. S. Dartevelle produced the Pjvk-G21 antibody. G.S. and S. Delmaghani performed the microarray experiments. I.P., J.D., and S. Delmaghani performed the cell biology experiments. N.T., M.T., M.L., S. Delmaghani, and S.S. performed the ultrastructural studies. S. Delmaghani, A.M., and A.E. performed the rescue experiments; M.B. and D.D. performed the ex vivo electrophysiology; and P.A. performed the in vivo electrophysiology analyses. T.Z., M.A., and E.S.V. studied the mitochondrial membrane potential. C.P., P.A., S. Delmaghani, J.D., and J.-P.H. wrote the manuscript.

ACKNOWLEDGMENTS

We thank M. Aghaie and M. Mobasheri for clinical data, V. Michel for immunohistolabeling, F. Langa-Vives (*Centre d'ingénierie génétique murine* platform) for $Pvjk^{fl/fl}$ mice engineering, J. Levilliers for her help in the preparation of the manuscript, J. Thornton and N. Furnham for protein structure prediction and analysis, and M. Ricchetti and P. Aubourg for fruitful discussions. This work was supported by the Louis-Jeantet Foundation, ANR-NKTH "HearDeafTreat" (2010-INTB-1402-23 01 and TÉT_10-1-2011-0421), Fondation Bettencourt Schueller, Fondation Agir pour l'Audition, Humanis Novalis-Taitbout, Réunica-Prévoyance, BNP Paribas, and the French state program ''Investissements d'Avenir'' (ANR-10-LABX-65) (to C.P.).

Received: April 24, 2015
Revised: August 2, 2015
Accepted: September 22, 2015
Published: November 5, 2015

REFERENCES

Ashmore, J. (2008). Cochlear outer hair cell motility. Physiol. Rev. *88*, 173–210.

Avan, P., Büki, B., and Petit, C. (2013). Auditory distortions: origins and functions. Physiol. Rev. *93*, 1563–1619.

Borck, G., Rainshtein, L., Hellman-Aharony, S., Volk, A.E., Friedrich, K., Taub, E., Magal, N., Kanaan, M., Kubisch, C., Shohat, M., and Basel-Vanagaite, L. (2012). High frequency of autosomal-recessive DFNB59 hearing loss in an isolated Arab population in Israel. Clin. Genet. *82*, 271–276.

Brown, K.D., Maqsood, S., Huang, J.Y., Pan, Y., Harkcom, W., Li, W., Sauve, A., Verdin, E., and Jaffrey, S.R. (2014). Activation of SIRT3 by the NAD^+ precursor nicotinamide riboside protects from noise-induced hearing loss. Cell Metab. *20*, 1059–1068.

Collin, R.W., Kalay, E., Oostrik, J., Caylan, R., Wollnik, B., Arslan, S., den Hollander, A.I., Birinci, Y., Lichtner, P., Strom, T.M., et al. (2007). Involvement of DFNB59 mutations in autosomal recessive nonsyndromic hearing impairment. Hum. Mutat. *28*, 718–723.

Delmaghani, S., del Castillo, F.J., Michel, V., Leibovici, M., Aghaie, A., Ron, U., Van Laer, L., Ben-Tal, N., Van Camp, G., Weil, D., et al. (2006). Mutations in the gene encoding pejvakin, a newly identified protein of the afferent auditory pathway, cause DFNB59 auditory neuropathy. Nat. Genet. *38*, 770–778.

Diano, S., Liu, Z.W., Jeong, J.K., Dietrich, M.O., Ruan, H.B., Kim, E., Suyama, S., Kelly, K., Gyengesi, E., Arbiser, J.L., et al. (2011). Peroxisome proliferation-associated control of reactive oxygen species sets melanocortin tone and feeding in diet-induced obesity. Nat. Med. *17*, 1121–1127.

Dobie, R.A. (2008). The burdens of age-related and occupational noise-induced hearing loss in the United States. Ear Hear. *29*, 565–577.

Ebberink, M.S., Koster, J., Visser, G., Spronsen, Fv., Stolte-Dijkstra, I., Smit, G.P., Fock, J.M., Kemp, S., Wanders, R.J., and Waterham, H.R. (2012). A novel defect of peroxisome division due to a homozygous non-sense mutation in the PEX11β gene. J. Med. Genet. *49*, 307–313.

Ebermann, I., Walger, M., Scholl, H.P., Charbel Issa, P., Lüke, C., Nürnberg, G., Lang-Roth, R., Becker, C., Nürnberg, P., and Bolz, H.J. (2007). Truncating mutation of the DFNB59 gene causes cochlear hearing impairment and central vestibular dysfunction. Hum. Mutat. *28*, 571–577.

Henderson, D., Bielefeld, E.C., Harris, K.C., and Hu, B.H. (2006). The role of oxidative stress in noise-induced hearing loss. Ear Hear. *27*, 1–19.

Housley, G.D., Morton-Jones, R., Vlajkovic, S.M., Telang, R.S., Paramananthasivam, V., Tadros, S.F., Wong, A.C., Froud, K.E., Cederholm, J.M., Sivakumaran, Y., et al. (2013). ATP-gated ion channels mediate adaptation to elevated sound levels. Proc. Natl. Acad. Sci. USA *110*, 7494–7499.

Imig, T.J., and Durham, D. (2005). Effect of unilateral noise exposure on the tonotopic distribution of spontaneous activity in the cochlear nucleus and inferior colliculus in the cortically intact and decorticate rat. J. Comp. Neurol. *490*, 391–413.

Kujawa, S.G., and Liberman, M.C. (2009). Adding insult to injury: cochlear nerve degeneration after "temporary" noise-induced hearing loss. J. Neurosci. *29*, 14077–14085.

Li, X., Baumgart, E., Dong, G.X., Morrell, J.C., Jimenez-Sanchez, G., Valle, D., Smith, K.D., and Gould, S.J. (2002). PEX11alpha is required for peroxisome proliferation in response to 4-phenylbutyrate but is dispensable for peroxisome proliferator-activated receptor alpha-mediated peroxisome proliferation. Mol. Cell. Biol. *22*, 8226–8240.

Lopez-Huertas, E., Charlton, W.L., Johnson, B., Graham, I.A., and Baker, A. (2000). Stress induces peroxisome biogenesis genes. EMBO J. *19*, 6770–6777.

Mizuno, Y., Kurochkin, I.V., Herberth, M., Okazaki, Y., and Schönbach, C. (2008). Predicted mouse peroxisome-targeted proteins and their actual subcellular locations. BMC Bioinformatics *9* (*Suppl 12*), S16.

Møller, A.R., and Jannetta, P.J. (1983). Interpretation of brainstem auditory evoked potentials: results from intracranial recordings in humans. Scand. Audiol. *12*, 125–133.

Ohlemiller, K.K., Wright, J.S., and Dugan, L.L. (1999). Early elevation of cochlear reactive oxygen species following noise exposure. Audiol. Neurootol. *4*, 229–236.

Oliver, D., Taberner, A.M., Thurm, H., Sausbier, M., Arntz, C., Ruth, P., Fakler, B., and Liberman, M.C. (2006). The role of BKCa channels in electrical signal encoding in the mammalian auditory periphery. J. Neurosci. *26*, 6181–6189.

Rice, M.E. (2011). H_2O_2: a dynamic neuromodulator. Neuroscientist *17*, 389–406.

Robles, L., and Ruggero, M.A. (2001). Mechanics of the mammalian cochlea. Physiol. Rev. *81*, 1305–1352.

Santos, M.J., Quintanilla, R.A., Toro, A., Grandy, R., Dinamarca, M.C., Godoy, J.A., and Inestrosa, N.C. (2005). Peroxisomal proliferation protects from beta-amyloid neurodegeneration. J. Biol. Chem. *280*, 41057–41068.

Schrader, M., and Fahimi, H.D. (2006). Peroxisomes and oxidative stress. Biochim. Biophys. Acta *1763*, 1755–1766.

Schrader, M., Bonekamp, N.A., and Islinger, M. (2012). Fission and proliferation of peroxisomes. Biochim. Biophys. Acta *1822*, 1343–1357.

Schwander, M., Sczaniecka, A., Grillet, N., Bailey, J.S., Avenarius, M., Najmabadi, H., Steffy, B.M., Federe, G.C., Lagler, E.A., Banan, R., et al. (2007). A forward genetics screen in mice identifies recessive deafness traits and reveals that pejvakin is essential for outer hair cell function. J. Neurosci. *27*, 2163–2175.

Smith, J.J., and Aitchison, J.D. (2013). Peroxisomes take shape. Nat. Rev. Mol. Cell Biol. *14*, 803–817.

Starr, A., and Rance, G. (2015). Auditory neuropathy. Handb. Clin. Neurol. *129*, 495–508.

Tang, X.D., Garcia, M.L., Heinemann, S.H., and Hoshi, T. (2004). Reactive oxygen species impair Slo1 BK channel function by altering cysteine-mediated calcium sensing. Nat. Struct. Mol. Biol. *11*, 171–178.

Wang, Y., Hirose, K., and Liberman, M.C. (2002). Dynamics of noise-induced cellular injury and repair in the mouse cochlea. J. Assoc. Res. Otolaryngol. *3*, 248–268.

Waterham, H.R., and Ebberink, M.S. (2012). Genetics and molecular basis of human peroxisome biogenesis disorders. Biochim. Biophys. Acta *1822*, 1430–1441.